Finite-difference anisotropic traveltimes and raypaths

Marco A. Perez and John C. Bancroft

ABSTRACT

Traveltimes are calculated using finite-difference solutions to the eikonal equation. The scheme presented computes traveltimes based on a finite-difference approximation to the eikonal equation for transversely isotropic (TI) and isotropic media. The method expands along wavefronts, following minimum traveltimes to honor causality. A technique for determining raypaths using the reciprocity principle is also presented. The proposed methods are valid for weak to moderate levels of anisotropy as defined by Thomsen's parameters.

INTRODUCTION

Both seismic imaging and inversion techniques are highly dependent upon the computation of accurate traveltimes of a geologic model. There are two basic methods that are commonly used to estimate traveltimes: raytracing and finite-difference approximations to the eikonal equation. Raytracing techniques are accurate and used quite frequently in the calculation of traveltimes, however they are unable to trace through shadow zones and locate true minimum traveltimes (Vidale, 1988). The alternative method is the finite-difference solution to the eikonal equation alleviating problems encountered in raytracing by calculating traveltimes at every grid point. However they can break down when encountering harsh velocity contrasts. This paper presents a 2-D, finite-difference, traveltime and ray-path calculator for TI media that can be employed in Kirchhoff migration and seismic tomography.

Vidale first introduced a finite-difference solution to the eikonal equation in 1988. However, this algorithm could not handle velocity contrasts greater than $V_2/V_1 > \sqrt{2}$ (Qin et al, 1992). Van Trier and Symes (1991), Podvin and Lecomte (1991), and Qin et al. (1992) subsequently modified this algorithm using different techniques attempting to honor causality in isotropic media. By honouring causality, these methods were able to overcome some of the velocity contrast problems encountered by Vidale as well as increasing the computation's accuracy. Dellinger (1991), Eaton (1993), and Lecomte (1993) extended the causal algorithms to address anisotropy. The scheme proposed in this paper customizes the expanding wavefront technique proposed by Qin et al. for a square-grid design. Eaton's hexagonal-grid method is similar to this scheme, but uses the elastic stiffness tensor to define anisotropy as opposed to the Thomsen parameters employed in this method. The proposed technique also exploits Huygens principle to account for refracted travel paths. The

ray paths for source-scatterpoint pairs are calculated based on the method described by Matsuoka and Ezaka (1992) and Asakawa and Kawanaka (1993).

THEORY

The proposed technique uses the algorithm proposed by Qin et al. that attempts to honour causality by expanding wavefronts along minimum traveltimes. Anisotropy is introduced by considering Thomsen's (1986) anisotropic parameters ($\varepsilon, \delta, \gamma, \alpha_0, \beta_0$), to be constant in each cell. Assuming plane-wave propagation, it follows that the angle dependent phase velocity, $V(\theta)$, can be computed once the unknown angle is determined. Once the phase velocity is defined, traveltimes can be estimated using the stencils originally defined by Vidale (1988).

Transverse isotropy

All media can be described by their appropriate elastic parameters. Isotropic media has two independent parameters, C_{11} and C_{44} that control P- and S-wave velocity. Three additional elastic parameters are required to define transversely isotropic media, C_{13}, C_{66}, and C_{33}. Adopting the Voigt recipe, TI media is represented in matrix form as

$$C_{\alpha\beta} = \begin{bmatrix} C_{11} & (C_{11}-2C_{66}) & C_{13} & & & \\ & C_{11} & C_{13} & & & \\ & & C_{33} & & & \\ & & & C_{44} & & \\ & & & & C_{44} & \\ & & & & & C_{66} \end{bmatrix} \tag{1}$$

Thomsen combines these elastic parameters to define a new set of parameters so as to determine their physical significance. P-wave propagation uses four of these parameters:

$$\alpha_0 = \sqrt{C_{11}/\rho} \tag{2}$$

$$\beta_0 = \sqrt{C_{44}/\rho}\,, \tag{3}$$

$$\varepsilon \equiv \frac{C_{11}-C_{33}}{2C_{33}} \tag{4}$$

and

$$\delta \equiv \frac{C_{66} - C_{44}}{2C_{44}}. \tag{5}$$

The first two parameters are the vertical P- and S-wave velocities while the last two parameters are a linear combination of the elastic constants. The parameter ε, controls the ratio between horizontal and vertical velocity while δ controls the near vertical anisotropy (Thomsen, 1986).

Wavefront propagation reflects the differences in elastic parameters between anisotropic an isotropic media. The raypath for anisotropic media is not orthogonal to the wavefront as it is for isotropic media is one of these differences.

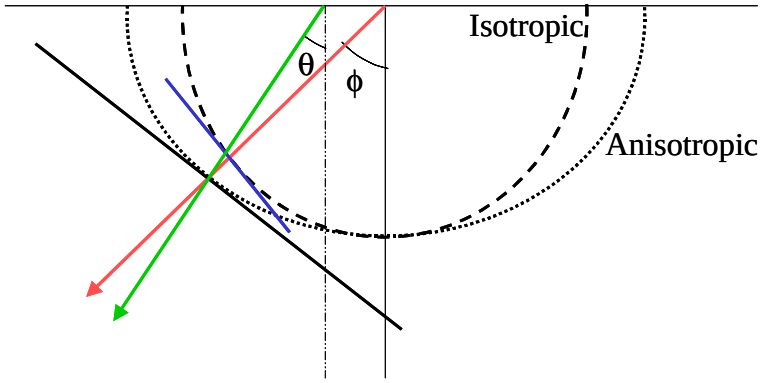

FIG. 1. Figure illustrating the difference between the group angle (ϕ) and the phase angle (θ). Finely dotted line is the transversely isotropic wavefront while the coarsely dotted line is isotropic.

Figure 1 shows two different paths taken to arrive at a single point. The path normal to the wavefront defines the phase velocity while the other path defines the group velocity.

The phase velocity will be used in determining traveltimes since the finite-difference solution to the eikonal equation assumes plane wave propagation. The phase velocity for transversely isotropic media using Thomsen's parameters is given by

$$V_P^2(\theta) = \alpha_0^2\left[1 + \varepsilon \sin^2\theta + D^*(\theta)\right] \tag{6}$$

where

$$D^*(\theta) \equiv \frac{1}{2}\left(1-\frac{\beta_0^2}{\alpha_0^2}\right)\left\{\left[1+\frac{4\delta^*}{\left(1-\beta_0^2/\alpha_0^2\right)}\sin^2\theta\cos^2\theta+\frac{4\left(1-\beta_0^2/\alpha_0^2+\varepsilon\right)\varepsilon}{\left(1-\beta_0^2/\alpha_0^2\right)}\sin^4\theta\right]^{1/2}-1\right\} \tag{7}$$

and

$$\delta^* \equiv \frac{1}{2C_{33}}\left[2\left(C_{13}+C_{44}\right)^2-\left(C_{33}-C_{44}\right)\left(C_{11}+C_{33}-2C_{44}\right)\right]. \tag{8}$$

Eikonal equation

The foundation of the traveltime method is the based on a finite-difference solution to the eikonal equation

$$\frac{1}{c^2}=\left(\frac{\partial\tau}{\partial x}\right)^2+\left(\frac{\partial\tau}{\partial z}\right)^2. \tag{9}$$

It is used as an approximation in calculating the traveltime through isotropic media given an appropriately defined velocity function. For anisotropic media, there is no succinct form of the eikonal equation. Instead, for the general anisotropic case, one must solve a sixth-order partial differential equation for τ,

$$\det\left|C_{ijkl}n_j n_l-\rho v^2\delta_{ik}\right|=0 \tag{10}$$

where C_{ijkl} is the elastic modulus tensor, n is the directional cosine of the wavefront normal, ρ is density and v is the wavefront normal velocity (Eaton, 1993). For the transversely isotropic case, the analytic solution is known for velocity and can be substituted into the isotropic eikonal equation giving the approximation

$$\frac{1}{c(\theta)^2}=\left(\frac{\partial\tau}{\partial x}\right)^2+\left(\frac{\partial\tau}{\partial z}\right)^2 \tag{11}$$

where velocity is a function of the propagation angle, θ.

Wavefront expansion stencils

The anisotropic modifications to the Qin et al scheme consist of determining the wavefront normal propagation direction. There are two stencils used, each of which require knowledge of the propagation direction. The first stencil uses three points of a

cell to determine the fourth. The schematic diagram in Figure 2 shows how this is accomplished.

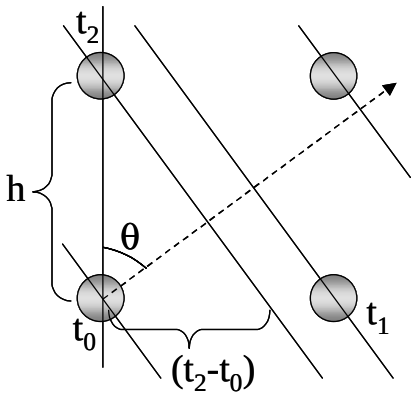

FIG. 2. Figure showing geometry for plane-wave angle determination. The variable h denotes the cell size, θ denotes the angle of propagation and t0, t1, t2 denote the known traveltimes with t0 < t1 < t2.

Given times t_0, t_1 and t_2 the slope of the line normal to the plane waves is

$$slope = \frac{\Delta z}{\Delta x} = \frac{h}{h\left(\frac{t_2 - t_0}{t_1 - t_0}\right)} = \left(\frac{t_1 - t_0}{t_2 - t_0}\right) \tag{12}$$

The arctangent of the slope is the propagation angle, thus establishing the velocity through which the cell is traversed. This velocity is then used in the extrapolation equation

$$t_3 = t_0 + \sqrt{2\left(hs(\theta)^2\right) - \left(t_2 - t_1\right)^2} \tag{13}$$

defined by Vidale (1988) to calculate the traveltime to the unknown point.

In cases where the points required to use equation (13) do not exist, a scheme based on Huygen's principle is used. To determine the traveltime to the unknown point shown in Figure 3, traveltimes are interpolated between t_1 and t_2.

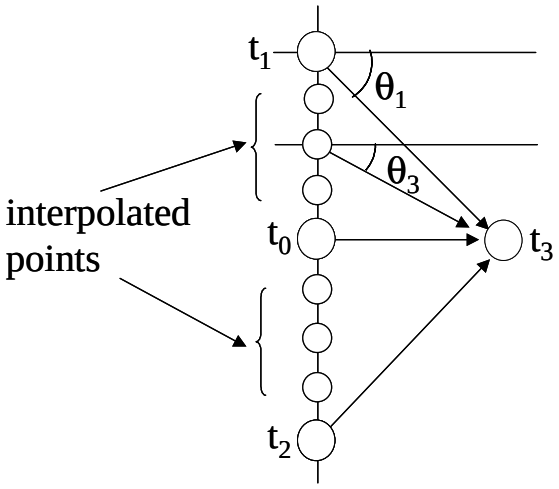

FIG. 3. Secondary method used to calculate traveltimes. Given the known traveltimes of t0, t1, and t2, intermediate traveltimes are determined via interpolation. Based on the location of the interpolated traveltimes, phase angles and traveltimes are computed. The minimum traveltime is kept within the estimation zone since it corresponds to the first arrival.

The phase angle of the plane wave is easily calculated since the positions of the points are known. The time to the unknown point is calculated using

$$t_{3i} = t_i + {}^{h_i}\!/_{V_p(\theta_i)} \tag{14}$$

where h_i is the distance from the *ith* interpolated point to the unknown point and V_i is the angle dependent velocity from the *ith* known point to the unknown point t_3. The minimum traveltime is chosen as the first arrival. The combined application of the stencils shown allows for the traveltime calculation of all grid points.

Wavefront expansion scheme

The traveltime method attempts to follow the manner in which a wavefront would expand. In general, the points on a grid are divided into three groups: accepted points, estimated points, and empty points. The accepted points are causally calculated traveltimes, the estimated points are traveltime estimates based on the accepted points and the empty points are those that have not come into contact with the computational front. The traveltimes of points surrounding the accepted points are estimated and the estimated point with the minimum traveltime becomes accepted. This process is repeated until all points in the grid have accepted traveltimes. In this way computation follows the wavefront expansion.

The expansion scheme begins with a source point (S), designated as an accepted point. Initially, Vidale's algorithm is used to calculate the horizontal and vertical grid points (A, B, C, D in Figure 4) surrounding the source. This method assumes that the plane-wave propagation angles are 0° and 90° with respect to vertical. Thomsen's

phase velocity ($V(\theta)$) equation is used to calculate the velocity at both propagation angles.

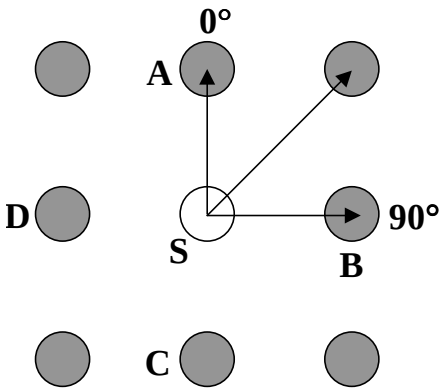

FIG. 4. Determination wavefront propagation angle from three known traveltime points which determines the angle dependent phase velocity.

The remaining points are calculated using equation (13). Given three computed traveltimes at points *A*, *B*, and *S*, the angle of propagation within the cell is determined. Thomsen's $V(\theta)$ is used in Vidale's approximation of the eikonal equation to calculate the traveltime to point *a*. The same procedure is followed to compute traveltimes at point's *b*, *c*, and *d*.

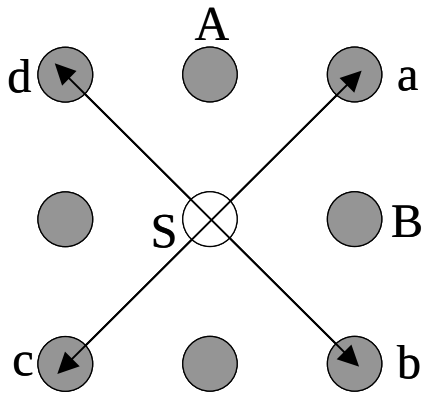

FIG. 5. Initial estimation points calculated using Vidale's plane-wave equation (13).

After this initial zone is computed, the minimum becomes an accepted point and a new estimation zone is constructed which surrounds the accepted points. The new estimation points are computed using the two stencils previously defined. From the new estimation zone, the minimum again becomes accepted and the process of constructing an estimation zone and choosing the minimum is repeated until all grid points become accepted points.

Raypath determination

The method proposed for approximating raypaths is based on the principle of reciprocity. This principle states that a ray follows the *minimum summed traveltime* path of the backward and forward propagation. Forward propagation consists of the traveltime from source to receiver while backward propagation is from receiver to the source. The previously described finite-difference method is used to solve for the forward propagating traveltimes. However, instead of computing a separate traveltime map for the receiver, the receiver is backward propagated to the source location using the traveltimes found from forward propagation. Within an isotropic cell, the location of the *minimum summed traveltime* of the corresponding source-receiver pair is established by the intersection of the normal to the plane waves, $V(\theta)$, and the cell boundary. The direction of the plane waves is computed using the forward propagation traveltimes and equation (14). This minimum is the new receiver location for the next cell (Figure 6). The receiver is backward propagated until it is collocated with the source.

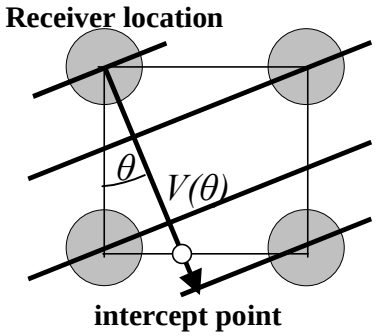

FIG. 6. The backward propagation method locates the intercept point between the phase velocity and the cell boundary to define the new receiver location for the next cell in isotropic media.

In anisotropic media, the raypath is not normal to the wavefronts (Figure 1). However, the ray angle (φ) can be computed from the phase angle (θ) and the known anisotropic parameters within the cell. Equations have been derived showing the relationship between group and phase angle (Brown et al, 1991).

$$\phi_p = \theta_p + \tan^{-1}\left[\frac{\varepsilon \sin 2\theta + \left(dD^*/d\theta_p\right)}{2\left(1+\varepsilon \sin^2\theta_p + D^*\left(\theta_p\right)\right)}\right] \tag{14}$$

Using the ray direction found by the ray angle, the intercept at the cell boundary can be determined.

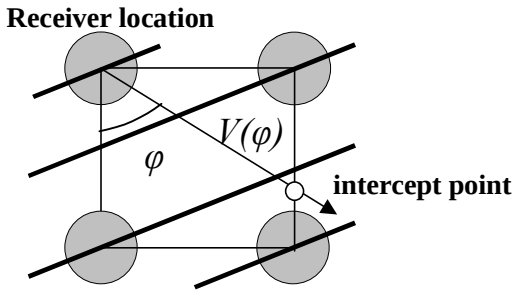

FIG. 7. The phase angle (θ) for an anisotropic cell can be estimated from three known traveltime grid nodes. The ray angle (φ) is then determined from the phase angle and anisotropy parameters. The intercept point is found at the intersection of $V(\varphi)$ and the cell boundary.

As well as determining the intersection point from the ray angle, the *minimum summed traveltime* is also compared to the rays that travel along the cell boundary. These rays correspond to the refracted part of the wavefront. The *minimum summed traveltime* of the refracted rays and the ray angle corresponds to the appropriate ray-path leading back to the source.

In backward propagating the receiver to the source, it is assumed that the traveltimes using the group and phase velocities are equivalent. For plane-wave propagation, it can be shown that using the group or phase velocity results in the same traveltime.

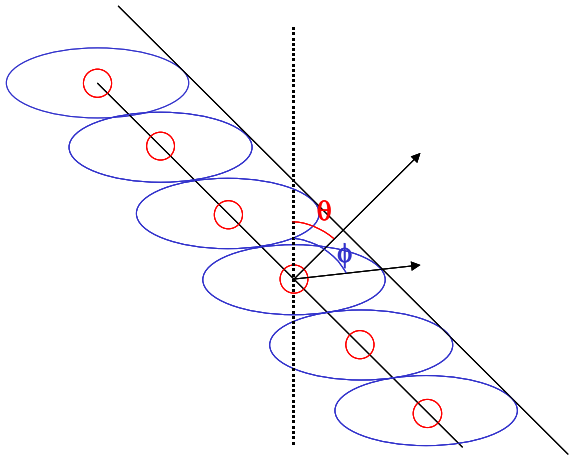

FIG. 8. Reconstruction of an anisotropic plane wave from secondary sources. Both group and phase velocities yield the same traveltime to the second plane wave.

In Figure 8, each circle represents a Huygen secondary point source of the wavefront. Each secondary source emits a wave defined by the group velocity that interferes constructively along the next plane wave shown. The intersection of the second plane wave and the secondary source wavelets show that the time required to reach the second plane wave can be computed by either using the group or phase velocity.

RESULTS

The traveltime scheme is tested on a simple homogeneous transversely isotropic velocity model. The model size contains 2500 cells each with dimensions of 10 metres. The following parameters were used to test traveltime accuracy

	α_0	β_0	δ	ε
Model 1 Weak anisotropy	3000 m/s	2000 m/s	0.05	0.1
Model 2 Moderate anisotropy	3000 m/s	2000 m/s	0.2	0.2

Table 1. Parameters used to test finite-difference traveltime scheme

Figure 9 shows the traveltime contours for the weakly transversely isotropic medium.

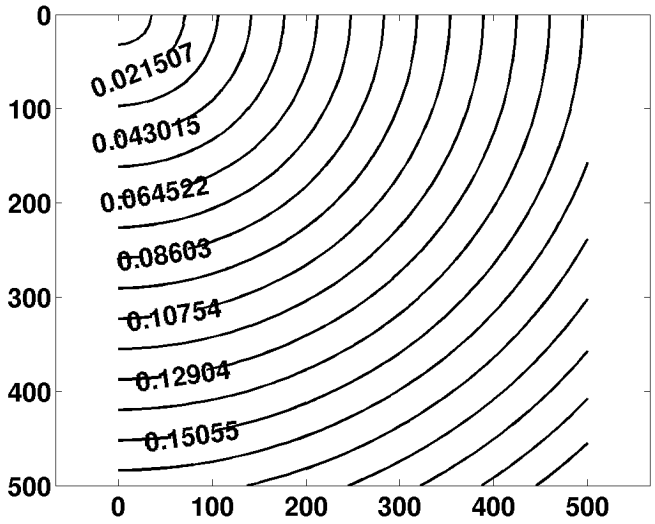

FIG. 9. Traveltime contours for a weakly anisotropic medium. Traveltime contour have units of seconds.

The error associated with this model, is seen in Figure 10. It follows that because the scheme is based on a plane wave approximation, areas along the wavefront with a large amount of curvature will not be as accurate. The asymmetry in the error plot also shows that there is anisotropy present within the model.

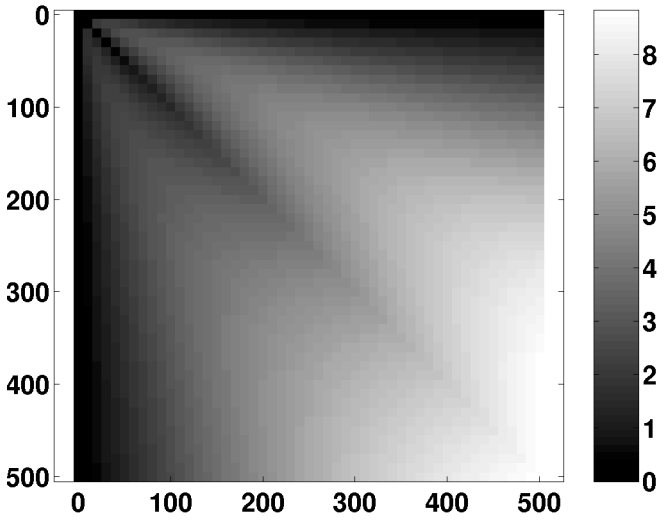

FIG. 10. Traveltime errors for weakly anisotropic medium whose contours are shown in Figure 9. Error bar has units of 10^{-4} seconds

Figure 11 shows the raypaths determined from the traveltimes shown in Figure 9. In anisotropic media, raypaths are straight and are correctly displayed in the figure below. The analytical rays are superimposed as a comparison.

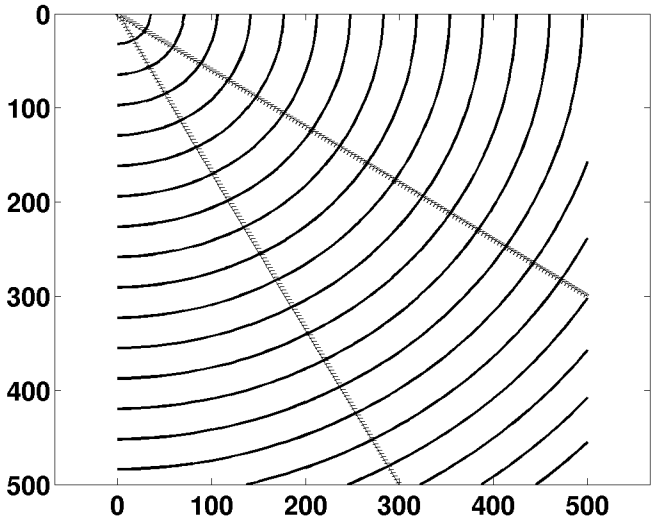

FIG. 11. Raypaths calculated using traveltime contours for a weakly anisotropic medium. Analytical raypaths are superimposed.

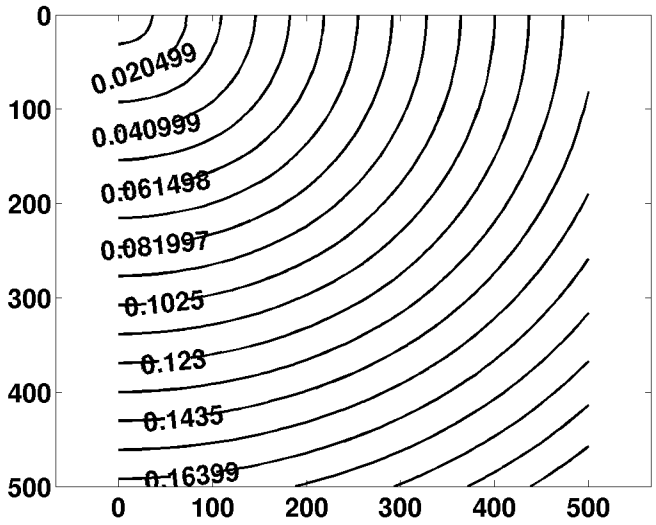

FIG. 12. Traveltime contours for a moderately anisotropic medium.

Figure 12 shows the traveltime contours for a moderate transversely isotropic medium.

Figure 13 shows the corresponding error. Notice that the amount of error has increased. This is a result of the wavefront curvature. In homogeneous isotropic media the wavefront is a part of a circle. In anisotropic media the wavefront will contain more plane like sections as well as areas with more curvature than there would exist in isotropic media. The error plot reflects this with the largest amount of error showing the part of the wavefront containing the largest amount of curvature.

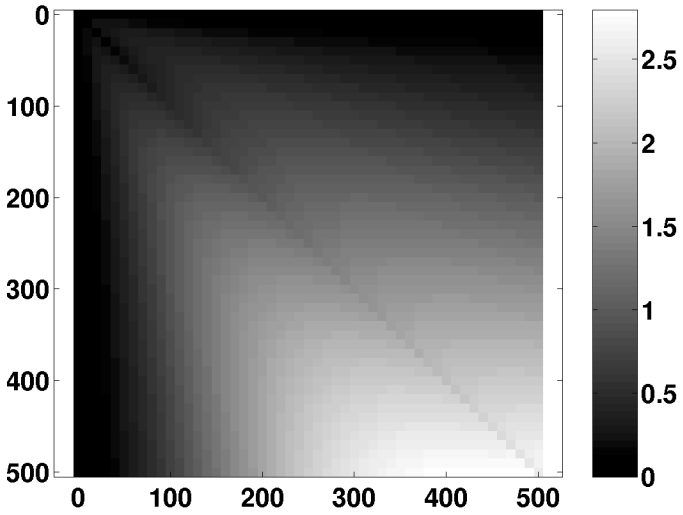

FIG. 13. Traveltime errors for moderately anisotropic medium whose contours are shown in Figure 12. Error bar has units of 10^{-3} seconds.

Figure 14 shows the raypaths for the moderate transversely isotropic medium. The analytical raypaths are plotted against the calculated raypaths for comparison.

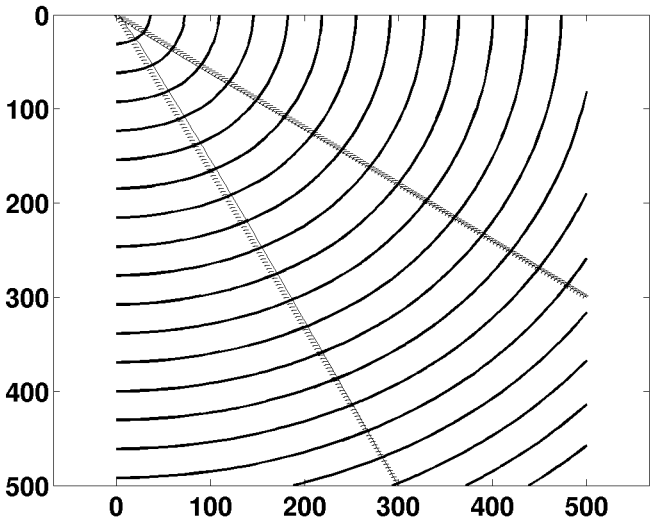

FIG. 14. Raypaths calculated using traveltime contours for a moderately anisotropic medium. Analytical raypaths are superimposed.

As can easily be seen, the left ray-path is less accurate than the right ray-path. This is counterintuitive since Figure 13 shows that the traveltimes of the latter raypath are less accurate. It follows that the reciprocity-based ray-path estimate is limited by the accuracy of forward traveltimes. Given that the plane waves cannot approximate a curved wavefront, it is expected that as the ray approaches the source, the quality of plane-wave estimate decreases. This is seen on the poorly approximated ray-path. Figure (15) shows how discretizing the wavefront as plane waves affects the raypaths.

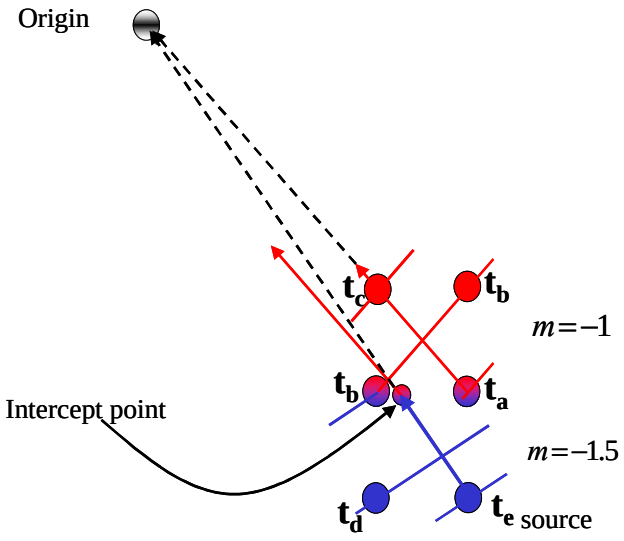

FIG. 15. Schematic illustrating how as the ray-path approaches the source of the plane waves, the ray-path approximation decreases.

However, it is not simply the traveltimes that determines the amount of ray-path error. The change in estimated ray-path curvature with respect to the actual change in ray-path curvature. In Figure 14, there is an estimated amount of ray-path curvature that does not exist. As a result, the ray-path estimation is incorrect.

The four following figures use the same model parameters defined in Table 2.

	α_0	β_0	δ	ε
Layer 1	4000 m/s	2000 m/s	0.0	0.0
Layer 2	3000 m/s	1500 m/s	0.2	0.2

Table 2. Parameter for 2-layer model.

Figure 16 shows the difference in raypaths when assuming isotropic media versus TI media. The traveltime contours were calculated using the correct anisotropic parameters. Both raypaths were calculated from the anisotropic traveltime contours.

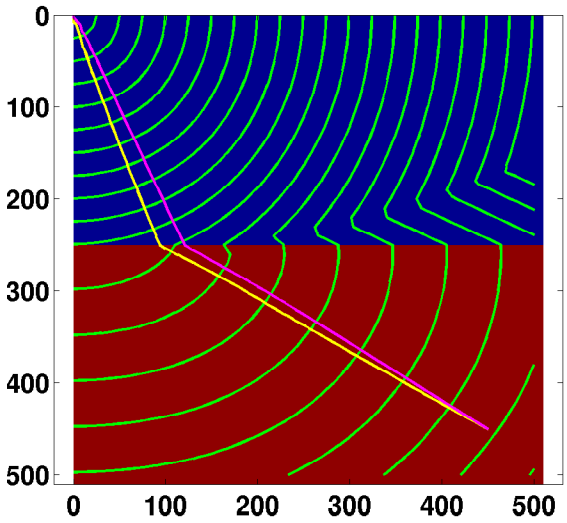

FIG. 16. Figure illustrating differences between the calculated isotropic and anisotropic raypaths using anisotropic traveltimes. Model parameters are seen in table 2.

The difference between the rays resides in deciding whether the traveltime contours are isotropic or anisotropic. The ray on the right assumes isotropic traveltimes and reflects this assumption since it is perpendicular to the wavefront. The left ray assumes TI media. Both raypaths have the same endpoints; however, the path taken is quite different. These differences can impact tomographic velocity analysis results.

The next three figures show how raypaths can be determined for a number of different acquisition geometries. Figure 17 displays VSP acquisition geometry, Figure 18 displays crosswell geometry, and Figure 19 displays a common reflection survey.

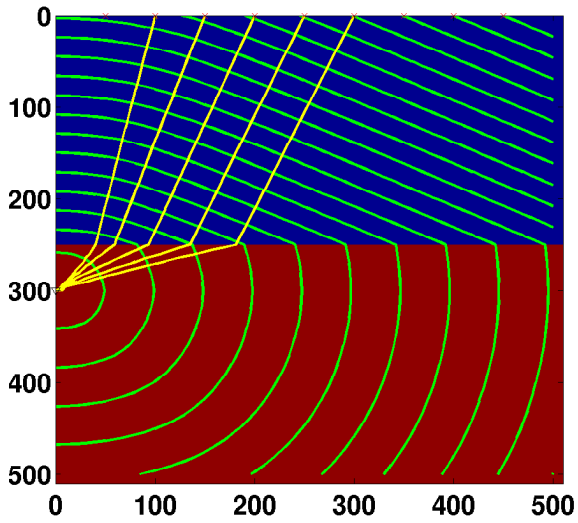

FIG. 17. VSP acquisition geometry

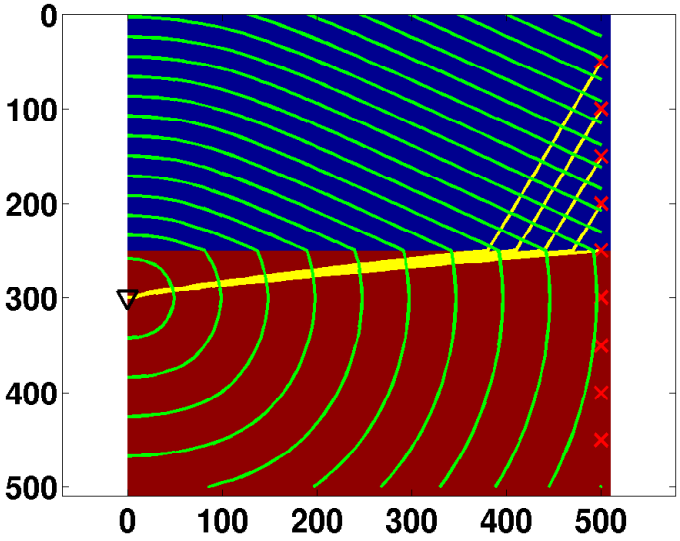

FIG. 18. Crosswell acquisition geometry

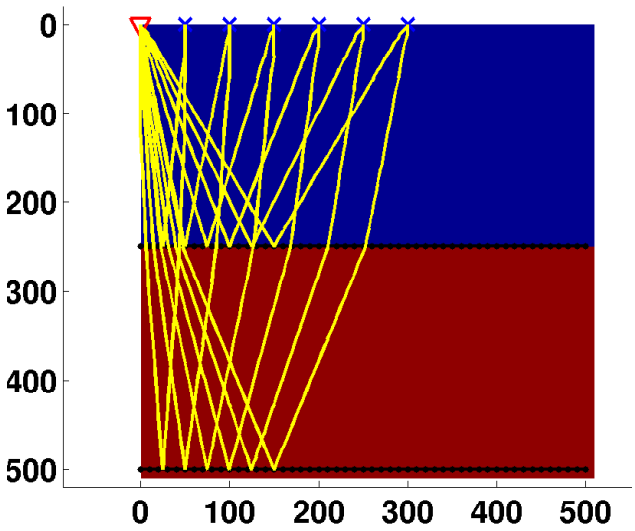

FIG. 19. Reflection survey acquisition geometry

These plots show the versatility of the method making the method simple to use for a wide range of applications.

CONCLUSIONS

The method presented is robust and efficient allowing for a wide range of applications. The technique is valid only for weak to moderate amounts of anisotropy and only calculates first arrivals. The accuracy of the algorithm is highest for plane waves and lowest when calculating traveltimes for wavefronts with a large amount of curvature.

Raypaths are determined based on the principle of reciprocity. Using the traveltime maps computed, the receiver is backward propagated to the source location. Raypaths are as accurate as the computed traveltimes. Since plane waves are used to approximate a curved wavefront, the raypaths calculated based on these assumptions exhibit errors when the approximation is a poor one. Because of the discrete nature of the calculation as the receiver approaches the source the quality of ray-path estimation decreases.

ACKNOWLEDGEMENTS

The authors would like to acknowledge the CREWES sponsors. The authors would also like to thank Jim Brown, Shauna Oppert and Pat Daley for useful discussions.

REFERENCES

Asakawa, E. and Kawanaka, T., 1993. Seismic raytracing using linear traveltime interpolation: Geophysical Prospecting, **41**, 99-111.

Brown, R.J., Lawton, D.C., and Cheadle, S.P., 1991. Scaled physical modelling of anisotropic wave propagation: multioffset profiles over and orthorhombic medium: Geophys. J. Int. **107**, 101-111.

Dellinger, J., 1991. Anisotropic finite-difference traveltimes: Soc. Expl. Geophys., 61st Annual Meeting.

Eaton, D.W.S., 1992. Finite-difference traveltime calculation for anisotropic media: Geophys. J. Int. **114**, 273-280.

Lecomte, I., 1993. Finite difference calculation of first traveltimes in anisotropic media: Geophys. J. Int., **113**, 318-342.

Matsuoka, T. and Ezaka, T., 1992. Raytracing using reciprocity: Geophysics, **57**, 326-333.

Perez, M.A. and Bancroft, J.C., 2000, Traveltime computation through isotropic media via the eikonal equation, CREWES Research Report **12**, 181-200.

Podvin, P. and Lecomte, I., 1991. Finite-difference computation of traveltimes in very contrasted velocity models: a massively parallel approach and its associated tools: Geophys. J. Int., **105,** 271-284.

Qin, F., Luo, Y.,K.B. Cai, W., and Schuster, G.T., 1992. Finite-difference solution to the eikonal equation along expanding wavefronts: Geophysics, **57**, 478-487.

Thomsen, L. 1986. Weak elastic anisotropy: Geophysics, **51**, 1954-1966.

Van Trier, J. and Symes, W.W., 1991. Upwind finite-difference calculation of traveltimes, Geophysics: **56**, 812-821.

Vidale, J., 1988, Finite-difference calculation of traveltimes: Bull. Seis. Soc. Am., **78**, 2602-2076.